CHIN. PHYS. LETT. Vol. 37, No. 11 (2020) 117501

Field- and Current-Driven Magnetization Reversal and Dynamic Properties of CoFeB-MgO-Based Perpendicular Magnetic Tunnel Junctions

Qingwei Fu(付清为)[1†], Kaiyuan Zhou(周恺元)[1†], Lina Chen(陈丽娜)[1], Yongbing Xu(徐永兵)[2], Tiejun Zhou(周铁军)[3*], Dunhui Wang(王敦辉)[3], Kequn Chi(迟克群)[4], Hao Meng(孟浩)[4], Bo Liu(刘波)[4], Ronghua Liu(刘荣华)[1,3*], and Youwei Du(都有为)[1,3]

[1]*National Laboratory of Solid State Microstructures, School of Physics and Collaborative Innovation Center of Advanced Microstructures, Nanjing University, Nanjing 210093, China*

[2]*York-Nanjing Joint Center (YNJC) for Spintronics and Nanoengineering, School of Electronics Science and Engineering, Nanjing University, Nanjing 210093, China*

[3]*Centre for Integrated Spintronic Devices, School of Electronics and Information, Hangzhou Dianzi University, Hangzhou 310018, China*

[4]*Key Laboratory of Spintronics Materials, Devices and Systems of Zhejiang Province, Hangzhou 311305, China*

(Received 31 July 2020; accepted 16 September 2020; published online 8 November 2020)

We report a perpendicular magnetic tunnel junction (pMTJ) cell with a tunnel magnetoresistance (TMR) ratio of nearly 200% at room temperature based on CoFeB/Ta/CoFeB as the free layer (FL) and a synthetic antiferromagnetic (SAF) multilayer [Pt/Co]/Ru/[Pt/Co]/Ta/CoFeB as the reference layer (RL). The field-driven magnetization switching measurements show that the pMTJs exhibit an anomalous TMR hysteresis loop. The spin-polarized layer CoFeB of SAF-RL has a lower critical switching field than that of FL. The reason is related to the interlayer exchange coupling (IEC) through a moderately thick Ta spacer layer among SAF-RLs, which generates a moderate and negative bias magnetic field on CoFeB of RL. However, the IEC among RLs has a negligible influence on the current-driven magnetization switching of FL and its magnetization dynamics.

PACS: 75.70.−i, 75.75.−c, 75.70.Cn, 75.75.Jn DOI: 10.1088/0256-307X/37/11/117501

Urgently demanded by ever-growing data storage, non-volatile spin-transfer torque magnetic random access memory (STT-MRAM) with the advancement of higher integration, higher speed and energy efficient, has received extensive advertences of both research and industry.[1−8] Both FL and RL of Ta/CoFeB/MgO-based pMTJ and high TMR ratio is currently considered as the most practical approach to exploit optimal STT-MRAM.[5,7−12] In an MTJ cell, the magnetization direction of the RL is fixed, whereas the magnetization of FL can be controlled by applying an electrical current based on the STT effect and achieve the data writing or logic operation.

In a conventional MTJ, FL usually suffers from the strong stray field generated by the adjacent ferromagnetic RL,[13] which causes severe asymmetry of STT-driven magnetization switching and consequently influences the logic operation of MRAM. At present, the SAF multilayer structure with the robust perpendicular magnetic anisotropy (PMA) as the RL has been wildly adopted. This SAF-RL usually consists of an SAF multilayer with a strong PMA as the pinned layer and an individual spin-polarized layer, CoFeB, which is coupled to the pinned layer SAF through a thin Ta layer due to IEC.[14] Except as the IEC spacer layer, Ta is also the indispensable seed layer of CoFeB in RL for achieving strong PMA. Therefore, the SAF-RL can not only minimize the stray field but also achieve a strong PMA and large coercive field H_c for the RL.[14,15] Although the SAF-RL possesses these advantages, the stiffness of IEC is finicky and highly sensitive to the thickness of the Ta layer, and its tiny deviation during the deposition process can result in a dramatic change of bias field and consequently change the coercive field H_c of the RL. Hence, to develop high-performance STT-RMAM, it is crucial to investigate whether IEC-induced bias field, which is related to the stiffness of IEC between the bottom SAF pinned layer and the top CoFeB spin-polarized layer in RL, will degrade the performance of STT-MRAM.[16−21]

In this Letter, we study magnetic field- and current-driven magnetization reversal characteristics

Supported by the National Key Research and Development Program of China (Grant No. 2016YFA0300803), the Open Research Fund of Jiangsu Provincial Key Laboratory for Nanotechnology, the National Natural Science Foundation of China (Grant Nos. 11774150 and 11874135), and the Natural Science Foundation of Jiangsu Province of China (Grant No. BK20170627).

†Qingwei Fu and Kaiyuan Zhou contributed equally to this work

*Corresponding authors. Email: rhliu@nju.edu.cn; tjzhou@hdu.edu.cn

© 2020 Chinese Physical Society and IOP Publishing Ltd

of the CoFeB/MgO-based pMTJ with a moderate stiffness of IEC between the bottom pinned SAF and adjacent spin-polarized CoFeB layer by TMR hysteresis loops, and the magnetic dynamical excitation as well as damping properties of the pMTJ by the spin-torque ferromagnetic resonance (ST-FMR) technique. We find an anomalous field-driven TMR hysteresis loop caused by a moderate and negative bias field on CoFeB RL due to the IEC among [Pt/Co]/Ta/CoFeB. However, it does not cause considerable influence on the current-induced STT magnetization switching of FL. Additionally, the field-frequency dispersion relation of pMTJ, obtained by the ST-FMR technique, demonstrates that three distinct resonance modes are related to standing spin-wave mode, uniform FMR mode, and edge mode of FL, respectively. The dynamics results further confirm that the IEC only affects the magnetization of RL rather than the magnetization reversal and dynamics of FL.

The pMTJ nano-pillar with three diameters (60, 70 and 80 nm) were fabricated based on the multilayer stacks of Ta (5)/Pt (5)/[Co (0.4)/Pt (0.4)]$_6$/Co (0.4)/Ru(∼0.9)/[Co (0.4)/Pt (0.4)]$_2$/Co(0.4)/Ta(0.55)/$Co_{20}Fe_{60}B_{20}$ (1)/MgO (0.9)/$Co_{20}Fe_{60}B_{20}$ (1.6)/Ta (0.43)/$Co_{20}Fe_{60}B_{20}$(1.0)/MgO(0.9)/Ta(5)/Ru(5). The numbers in parentheses are the thicknesses in nm, and the subscript of Co/Pt multilayers is the stacking number. The multilayer films were deposited under ∼3 mTorr Ar in a high vacuum physical vapor deposition system with base pressure less than 2×10^{-8} Torr. The metallic layers were deposited by DC magnetron sputtering, and the MgO was deposited by RF sputtering. The studied MTJ nano-pillars were nanofabricated by combing photolithography and ion beam milling technique. Figure 1(a) shows the stack structure of our pMTJs. The [Co/Pt] multilayers are coupled in antiferromagnetic by the Ru spacer layer and form a pinned SAF structure. The CoFeB(1), as the spin-polarized layer, couples with the SAF [Co/Pt] through 0.55 nm Ta spacer.

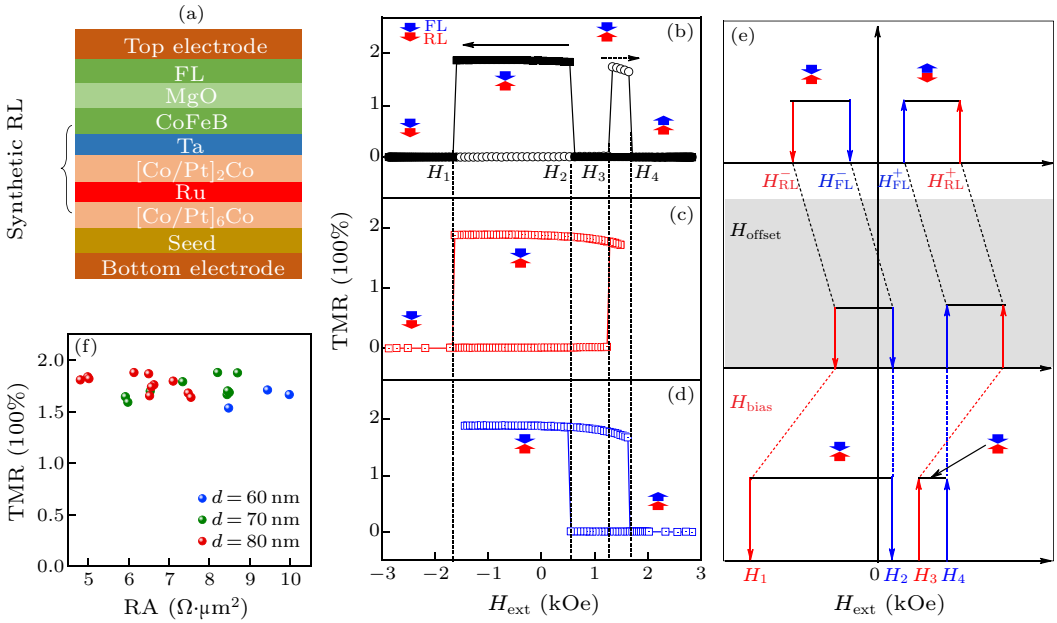

Fig. 1. TMR vs H_{ext} curves of MTJ. (a) Schematic of the sample stack. (b)–(d) TMR hysteresis major loop (b) and minor loop (c)–(d) of the MTJ with 60 nm diameter. The black arrows in (b) indicate the scanning direction of H_{ext}. (e) Typical TMR hysteresis loop of a standard MTJ (top panel), the whole hysteresis loop shifting along the positive external field (middle panel), and the IEC-induced negative bias field driven RL shifting (bottom panel). The bold arrows indicate the magnetization direction of the FL (blue) and RL (red), respectively. (f) Dependence of TMR ratios on resistance area (RA) for three different diameters pMTJs.

Firstly, the TMR hysteresis loops were investigated substantially under out-of-plane magnetic fields with a small I_{dc} of 1 μA. Figure 1(b) shows the representative major TMR hysteresis loops. The sharp TMR and a nearly steady high resistance state indicate that the pMTJ has a well-defined PMA for both RL and FL. The TMR ratio is defined as $\mathrm{TMR} = 100\% \times (R_{AP} - R_P)/R_P$, where R_P and R_{AP} are the resistances in the parallel (P) and antiparallel (AP) magnetization alignments of RL and FL, respectively. The pMTJ has a TMR ratio of as high as 188% at room temperature (RT), indicating the good quality of our samples. However, the major loop exhibits an asymmetric characteristic with one negative switching field H_1 and three positive switching fields H_2, H_3, H_4 [Fig. 1(b)], suggesting that the RL and/or FL would have anomalous magnetization reversal processes. To further explore the original physics behind

the asymmetric TMR curves, we performed two additional minor loops measurements below the maximum switching field H_4 and above the negative switching field H_1 ranges, respectively. Figure 1(c) shows that the minor loop has two specific switching fields corresponding to the H_1 and H_3 of the major loop, respectively. The $R_{\rm P}$ state indicates that the magnetizations of RL and FL both follow the external magnetic field $H_{\rm ext}$ and point down at $H_{\rm ext} < H_1$, while the $R_{\rm AP}$ state means that the magnetization of RL switches to point-up at the moderate H_3 and becomes antiparallel with FL as $H_{\rm ext}$ increases to H_3 from below H_1. While another minor TMR loop obtained above H_1 range, shown in Fig. 1(d), exhibits two switching fields corresponding to the H_2 and H_4 of the major loop, respectively. The $\rm R_P$ state is observed during $H_{\rm ext}$ scanning to near H_2 from above $H_4 = 1.71$ kOe, which indicates that the magnetizations of RL and FL are in a parallel state, and both point up. Then the MTJ is switched into the $R_{\rm AP}$ state at H_2 as the magnetization of FL is driven to point down by the external field and becomes antiparallel with RL. Based on the above analysis of the major and minor loops, we can identify that the TMR transitions occurred at the four critical fields H_1, H_2, H_3 and H_4 of the major loop correspond to magnetization switching of RL, FL, RL and FL, respectively, while in contrast to the standard reversal sequences (RL, FL, FL and RL) usually observed at TMR curves of conventional MTJ.

To better understand the crossover behavior of critical switching fields between RL and FL, we propose a simple model that can successfully describe the magnetization reversal processes of our MTJ device with only considering the IEC between SAF and adjacent CoFeB-RL and the stray field. Since the SAF with strong PMA is separated from the adjacent CoFeB-RL by the thin Ta layer in our MTJs, the IEC between SAF and RL originating from the RKKY effect is expected to induce an interface exchange bias (IEB) effect on the CoFeB-RL and dramatically shift its critical field down to below that of FL. To reproduce the complex TMR curves observed in Fig. 1(b), we used the schematic to illustrate how the major TMR vs $H_{\rm ext}$ loop evolves to the observed asymmetry loop from the standard TMR loop. One would expect that the critical switching fields of both RL and FL without stray field and exchange bias field should be symmetric to the external magnetic field, as shown at the top panel of Fig. 1(e). However, in practical nanoscale MTJ devices, many experiments show that the stray field can be dramatically suppressed but cannot be eliminated entirely by using the SAF-RL rather than using the FM-RL. Although the asymmetric TMR loop, as shown in the middle panel of Fig. 1(e), can be driven by an offset field ($H_{\rm offset}$) due to the stray field,[22–24] this offset field cannot induce the crossover behavior between the switching fields of RL and FL because the global stray field is expected to have the same effect on RL and FL based on structure analysis of the MTJs. As mentioned above, IEC between RL and SAF can exert an interlayer exchange bias field on RL under the RKKY mechanism and only uniaxially shift the coercivity of RL due to the fixed SAF. In contrast to the stray field, the TMR loop further shows that IEC-induced $H_{\rm bias}$ is opposite to $H_{\rm ext}$ and $H_{\rm offset}$ [Fig. 1(e)]. Therefore, the switching field H_4 of FL can be higher than that of RL H_3 due to IEC-induced negative $H_{\rm bias}$ on RL. Based on the above analysis, the experimentally observed anomalous magnetization reversal can be reproduced qualitatively, as shown in the bottom panel of Fig. 1(e).

Furthermore, we can quantitatively evaluate $H_{\rm offset}$ and $H_{\rm bias}$ by comparing the analysis of the experimental data and our proposed model. The four critical switching fields H_1, H_2, H_3 and H_4 are -1.65, 0.63, 1.25 and 1.71 kOe, respectively. Based on the above analysis, the four critical switching fields follow the following equations:

$$H_1 = H_{\rm RL}^{-} - H_{\rm bias} + H_{\rm offset}, \tag{1}$$

$$H_3 = H_{\rm RL}^{+} - H_{\rm bias} + H_{\rm offset}, \tag{2}$$

$$H_2 = H_{\rm FL}^{-} + H_{\rm offset}, \tag{3}$$

$$H_4 = H_{\rm FL}^{+} + H_{\rm offset}, \tag{4}$$

where $H_{\rm RL}^{-} = -H_{\rm RL}^{+}$ and $H_{\rm FL}^{-} = -H_{\rm FL}^{+}$ are the coercivity of the isolated RL and FL, respectively. $H_{\rm bias} = 1.37$ kOe and $H_{\rm offset} = 1.17$ kOe can be extracted easily by solving Eqs. (1)–(4).

Besides asymmetric characteristics of the switching fields, the TMR ratio also exhibits a slight unidirectional decrease in both major and minor TMR loops when $H_{\rm ext}$ approaches $H_{\rm FL}^{+}$, as shown in Figs. 1(b)–1(d). This small deviation from square shape may arise from the inhomogeneous PMA of FL or degradation of magnetization at the edge of MTJ pillar during the nano-fabrication processes. One should note that the interfacial Dzyaloshinskii–Moriya interaction (iDMI) existing in the interface between heavy metal and FM can induce an effective chiral field, which may also have an influence on magnetization reversal processes in a unidirectional way. Figure 1(f) shows TMR ratios of two dozen pMTJs with three different diameters (60, 70, and 80 nm). All studied samples have a high TMR ratio (150–200%) and do not show a clear dependence of TMR on the resistance area product (RA). Meanwhile, the RA of all samples is less than $10\,\Omega{\cdot}\mu{\rm m}^2$, indicating that our pMTJ array has good uniformity.

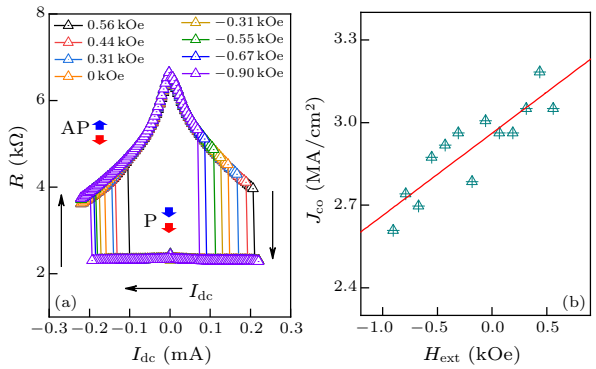

Fig. 2. Current-driven magnetization reversal characteristics of pMTJ with 60 nm diameter. (a) R vs I_{dc} loops under different out-of-plane fields H_{ext} from 0.56 to −0.90 kOe, respectively. Black arrows indicate the sweeping direction of I_{dc}. The bold arrows indicate the magnetization directions of FL and RL, respectively. (b) J_{c0} vs H_{ext}. The solid line is the fitting curve of Eq. (5).

The current-driven magnetization switching experiments were further performed at RT to investigate the STT switching of pMTJs. Figure 2(a) shows the representative R–I curves of pMTJ obtained by scanning I_{dc} at different out-of-plane magnetic fields varied from −0.90 to 0.56 kOe. The R_{AP} shows a noticeable decrease with increasing amplitude of current for all R–I curves. Additionally, the critical current $I_c^{AP\to P}$ (from AP state to P state) is less (larger) than $I_c^{P\to AP}$ (from P state to AP state) when applied a negative (positive) magnetic field. The strong current-dependent TMR ratio and field-dependent critical current (I_c) behaviors observed in Fig. 2(a) are quite consistent with previous reports.[25] The average critical switching current density $J_{co} = (J_c^{AP\to P} - J_c^{P\to AP})/2 = 3.0\,\mathrm{MA/cm^2}$ at zero external field is comparable to other CoFeB/MgO-based MTJs.[12,14,23] Based on Slonczewski's model of STT, J_{co} is quantitatively given by[26,27]

$$J_{co} = \left(\frac{2e}{\hbar}\right)\frac{\alpha M_S t(H_{ext} + M_{eff})}{\eta}, \tag{5}$$

where e is the electron charge, $\hbar$ is the reduced Planck constant, η, α, M_S, M_{eff} and t are the spin-transfer efficiency, Gilbert damping factor, saturation magnetization, effective magnetization, and thickness of the free layer, respectively. Spin-transfer efficiency is an essential parameter for STT-MRAM, which ($\eta = 0.29$) can be extracted by fitting the external field-dependent J_{co}, as shown in Fig. 2(b), with Eq. (5) and material parameters $t = 2.5\,\mathrm{nm}$, $M_S = 1000\,\mathrm{emu/cm^3}$ and $\alpha = 0.015$, where α and M_{eff} were obtained from our ST-FMR experiments, as discussed in the following. The tunnel spin polarization p was also estimated to be ∼70% from η by the Slonczewski method and approximately equal to the value directly calculated using the formula $p = [\mathrm{TMR}/(2+\mathrm{TMR})]^{1/2} = 69\%$.[26]

Based on both field-driven and current-driven magnetization reversal experiments, we found that the moderate IEC between SAF and RL significantly shifts the critical switching field of CoFeB-RL, whereas has a negligible influence on current-induced STT switching performance of the FL.

Beyond the discussion of the field- and STT-driven quasi-static magnetization reversal, the ST-FMR technique can also be utilized to characterize the physical properties of nanoscale pMTJ, such as magnetic damping. To obtain a better signal-to-noise ratio, we performed the ST-FMR measurements of 60 nm diameter pMTJ by scanning H_{ext} perpendicular to the device. Since the magnetization configurations of RL and FL are too complicated during the entire major loop, ST-FMR was only measured at the antiparallel state [Fig. 3(a)]. The ST-FMR spectra were well fitted by the sum of symmetric and antisymmetric Lorentzians,[28]

$$V_{dc} = V_A\frac{4(H_r - H_{ext})\Delta H}{4(H_r - H_{ext})^2 + \Delta H^2} + V_S\frac{\Delta H^2}{4(H_r - H_{ext})^2 + \Delta H^2} + V_{offset}, \tag{6}$$

where ΔH represents the full width at half maximum of the spectrum, H_r the resonant magnetic field, V_S and V_A the amplitudes of symmetric and antisymmetric Lorentzian, respectively. Figure 3(b) shows the dispersion relation between frequency and resonant magnetic field H_r. The resonance frequencies of the three modes decrease as H_{ext} increases, indicating that the corresponding total effective magnetization decreases with increasing H_{ext}. Since the FL (RL) magnetization direction is antiparallel (parallel) to the external field based on the minor TMR loop characteristics shown in Fig. 1(d), the effective magnetization of FL (RL) should decrease (increase) with increasing external field. Therefore, these modes are identified as the dynamical modes of the FL.[29] Additionally, no excitation mode related to the RL is observed in the pMTJs, indicating that the RL has been pinned effectively by bottom SAF due to IEC, which is different from the previously reported results of the MTJ without IEC where the RL can excite some dynamical modes.[29–31] The excitation mode of the RL in our pMTJ may be suppressed or shifted out of our study frequency range by the IEC-induced anisotropy.

Furthermore, it is necessary to identify the excitation type of these modes. In principle, the uniform magnetization precession possesses the strongest signal because FMR excitation extends to the whole magnetic area, suggesting that the center robust mode is likely in the uniform FMR mode. For the perpen-

dicularly magnetized system, the FMR dispersion relation follows the Kittle formula[29,32]

$$f = -\gamma(H_{\rm r} + M_{\rm eff}), \tag{7}$$

where $\gamma/2\pi = 29\,\text{GHz/T}$ is the gyromagnetic ratio and $M_{\rm eff} = 4\pi M_{\rm S} - H_{\rm offset} - H_{\rm K}$ the effective magnetization, $H_{\rm offset}$ the stray field, $M_{\rm S}$ the saturation magnetization and $H_{\rm K}$ the anisotropic field of the FL. To further confirm the above speculation, the experimental data (center mode) is quantitatively analyzed using the above Kittle formula. Figure 3(b) shows that the center FMR mode can be well fitted with Eq. (7) and fitting parameters $M_{\rm S} = 1000\,\text{emu/cm}^3$, $H_{\rm offset} = 1.17\,\text{kOe}$ and $H_{\rm K} = 10.85\,\text{kOe}$, consistent with material parameters of CoFeB in many previous reports. Besides the primary FMR mode, the two secondary excitation modes with a higher or lower frequency are also observed in our ST-FMR measurements. The spectra intensity of the high-frequency mode shows a distinct increase as the external field approaching to $H_{\rm FL}^{+}$ [Fig. 3(c)], which is closely related to the TMR ratio decreasing as observed in Fig. 1(d). As discussed above, the decrease of TMR ratio near $H_{\rm ext}$ approaching to $H_{\rm FL}^{+}$ is likely contributed from the magnetization tilt of the FL from the normal direction at the edge of MTJ nano-pillar under the opposite magnetic field. Therefore, the high-frequency mode is more likely the spin-wave mode localized at the edge of nano-pillar. Additionally, the confined standing spin-wave modes can also be excited in the pMTJ devices according to the previous experimental results reported by Safranski *et al.*[29] The dispersion relation of the fundamental standing spin wave can be expressed as[29]

$$\hbar(\omega_1 - \omega_0) = D(s/d)^2, \tag{8}$$

where ω_1 and ω_0 are the angular frequencies of the standing spin wave and FMR, respectively, $s = 3.6$ a numerical factor, d the diameter of pMTJ cell, and D the exchange stiffness. The frequency vs resonance field $H_{\rm r}$ curves of the two standing modes were fitted using Eq. (8), as shown in Fig. 3(b). For the low-frequency mode, the fitting parameter exchange stiffness D is $0.2\,\text{eV}\cdot\text{Å}^2$, consistent with the exchange stiffness range of 0.2–0.6 $\text{eV}\cdot\text{Å}^2$ of the CoFeB film.[33] However, the exchange stiffness of the high-frequency mode ($0.16\,\text{eV}\cdot\text{Å}^2$) was much beyond the exchange stiffness range of the studied film, further suggesting that it belongs to an edge spin-wave mode again.

From the above discussion about current-driven magnetization switching, Gilbert damping factor α plays a crucial role in determining the spin-transfer efficiency η of the STT switching performance.[25,34,35] Based on a linear relationship between the linewidth ΔH and FMR frequency f as follows:[35]

$$\Delta H = \Delta H_0 + \frac{2\pi\alpha f}{\gamma}, \tag{9}$$

where ΔH_0 is the extrinsic inhomogeneous linewidth, and $\gamma/2\pi = 29\,\text{GHz/T}$ the gyromagnetic ratio, we can extract the damping constant α from our ST-FMR experimental data, as shown in Fig. 3(e). The damping constant $\alpha = 0.015$ is comparable with the reported values in CoFeB-based pMTJ without IEC.[36]

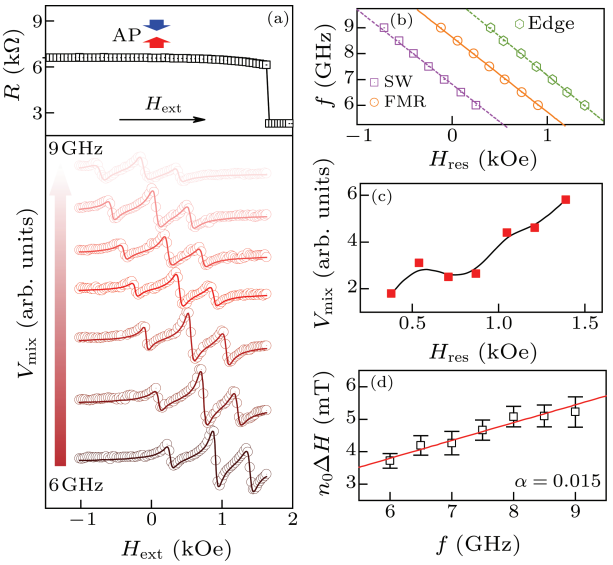

Fig. 3. (a) ST-FMR spectra and corresponding magnetoresistance curve of the pMTJ. The black and color arrows are the same as defined in Fig. 1. All spectra (bottom panel) are obtained at the $R_{\rm AP}$ state. (b) f vs $H_{\rm res}$ dispersion relations of different modes. The solid lines are fitting curves with the Kittle formula. (c) Dependence of ST-FMR signal on $H_{\rm res}$ of the edge mode. (d) Linewidth vs resonance frequency of FMR mode of FL. The solid line is the linear fitting using Eq. (9) with a damping constant $\alpha = 0.015$.

In summary, we have investigated the field- and current-driven magnetization reversal and dynamical excitation in pMTJs with an SAF multilayer structure as the RL. Combining the experimentally observed asymmetric field-driven TMR loops, the crossover behavior between FL and RL switching fields and the analytical model, we have demonstrated that a moderate IEC stiffness between CoFeB of RL and [Pt/Co] through a 0.55-nm-thick Ta spacer results in a negative bias field of $H_{\rm bias} = -1.37\,\text{kOe}$ on CoFeB of RL. The IEC-induced $H_{\rm bias}$ drags the coercivity of RL down to $H_3 = 1.25\,\text{kOe}$, being smaller than $H_4 = 1.71\,\text{kOe}$ of FL. The observed field-driven anomalous magnetization reversal sequences could be used to develop the multi-level magnetic logic devices. Furthermore, the results of current-driven magnetization switching and dynamics indicate that the IEC among RL has a negligible influence on the current-induced

STT effect on FL and its critical switching current. Our results provide an essential clue to design and fabricate high-performance STT-MRAM devices.

References

[1] Yu G *et al.* 2014 *Nat. Nanotechnol.* **9** 548
[2] Li Z P *et al.* 2016 *Appl. Phys. Lett.* **109** 182403
[3] Watanabe K *et al.* 2018 *Nat. Commun.* **9** 663
[4] Rehm L *et al.* 2019 *Appl. Phys. Lett.* **115** 182404
[5] Chatterjee J *et al.* 2019 *Appl. Phys. Lett.* **114** 092407
[6] Shadman A and Zhu J G 2019 *Appl. Phys. Lett.* **114** 022403
[7] Chen C H, Cheng Y H, Ko C W and Hsueh W J 2015 *Appl. Phys. Lett.* **107** 152401
[8] Yakushiji K *et al.* 2017 *Appl. Phys. Lett.* **110** 092406
[9] Lourembam J *et al.* 2018 *Appl. Phys. Lett.* **113** 022403
[10] Pathak S, Cha J, Jo K, Yoon H and Hong J 2017 *Appl. Phys. Lett.* **110** 232401
[11] Hämäläinen S J *et al.* 2017 *Phys. Rev. Appl.* **8** 014020
[12] Sato H *et al.* 2014 *Appl. Phys. Lett.* **105** 062403
[13] Choi G M, Shin I J, Min B C and Shin K H 2010 *J. Appl. Phys.* **108** 073913
[14] Sato H *et al.* 2013 *IEEE Trans. Magn.* **49** 4437
[15] Liu Y, Yu J and Zhong H 2019 *J. Magn. Magn. Mater.* **473** 381
[16] Meiklejohn W H and Bean C P 1956 *Phys. Rev.* **102** 1413
[17] Nogués J *et al.* 2005 *Phys. Rep.* **422** 65
[18] Meiklejohn W H 1962 *J. Appl. Phys.* **33** 1328
[19] Bollero A *et al.* 2006 *Appl. Phys. Lett.* **89** 152502
[20] Vinai G *et al.* 2014 *Appl. Phys. Lett.* **104** 162401
[21] Teichert N *et al.* 2015 *Appl. Phys. Lett.* **106** 192401
[22] Fuchs G D *et al.* 2005 *Appl. Phys. Lett.* **86** 152509
[23] Diao Z *et al.* 2005 *Appl. Phys. Lett.* **87** 232502
[24] Huai Y, Pakala M, Diao Z and Ding Y 2005 *Appl. Phys. Lett.* **87** 222510
[25] Wen Z *et al.* 2014 *Phys. Rev. Appl.* **2** 024009
[26] Slonczewski J C 2005 *Phys. Rev. B* **71** 024411
[27] Sun J Z 2000 *Phys. Rev. B* **62** 570
[28] Sankey J C *et al.* 2006 *Phys. Rev. Lett.* **96** 227601
[29] Safranski C J, Chen Y J, Krivorotov I N and Sun J Z 2016 *Appl. Phys. Lett.* **109** 132408
[30] Auerbach E, Leder N, Gider S and Arthaber H 2018 *IEEE Trans. Magn.* **54** 1
[31] Dohi T, Kanai S, Matsukura F and Ohno H 2017 *Appl. Phys. Lett.* **111** 072403
[32] de Loubens G *et al.* 2009 *Phys. Rev. Lett.* **102** 177602
[33] Yamanouchi M *et al.* 2011 *IEEE Magn. Lett.* **2** 3000304
[34] Zhang L, Fang B, Cai J and Zeng Z 2018 *Appl. Phys. Lett.* **112** 242408
[35] He C *et al.* 2018 *Phys. Rev. Appl.* **10** 034067
[36] Enobio E C I *et al.* 2015 *IEEE Magn. Lett.* **6** 1